The Mei-Yu Season Over the Taiwan Area

Yi-Leng Chen[a], **and Chuan-Chi Tu**[b], [a] Department of Atmospheric Sciences, University of Hawaii at Manoa, Honolulu, HI, United States and [b] Department of Atmospheric Sciences, National Central University, Zhongli, Taiwan

Synopsis

This article gives an overview of the seasonal, large-scale, synoptic, mesoscale, and island-scale circulations and front-terrain interactions during the Mei-Yu season over Taiwan.

The Mei-Yu jet/front over southern China exhibits baroclinic characteristics with thermally direct circulation across the frontal zone. When moisture transport from the northern South China Sea to the Taiwan area by the Marine Boundary Layer Jet occurs, conditions are favorable for widespread heavy rainfall over Taiwan.

Over the Taiwan area, front-terrain interactions, localized convergence, orographic blocking, lifting of the southwesterly flow, and local circulations during the diurnal cycle affect the timing and location of localized heavy precipitation.

Key Points

- An overview of the seasonal, large-scale, synoptic, and mesoscale circulations during the Mei-Yu season over Taiwan.
- Define the onset and ending of the Mei-Yu season over Taiwan.
- Lee cyclogenesis and development of the southwest vortices behind the high mountains during the approach of a shortwave trough in the westerlies.
- During the passage of a mid-latitude trough, continental cold air is advected southward behind the mid-latitude trough.
- Mei-Yu jet/front systems exhibit baroclinic characteristics.
- Decrease in the depth of the post-frontal cold air as the Mei-Yu front penetrates to the subtopics and the Taiwan area.
- The marine boundary layer jet plays a critical role in transporting moisture from the northern South China Sea to the Taiwan area.
- Heavy rainfall over the Taiwan area is localized in nature and related to front/terrain interactions, orographic lifting, localized low-level convergence and local circulations during the diurnal heating cycle.

Introduction

During the early summer rainy season of east Asia, a broad range of circulations with different spatial and time scales exist. This article describes the Mei-Yu season over Taiwan including the onset, ending, large-scale circulation patterns, transient disturbances, characteristics of Mei-Yu Jet/front systems, and moisture transport from the northern South China Sea to Taiwan. Over the Taiwan area, the postfrontal cold air is rather shallow at ~ 1 km. The role of front-terrain interactions, effects of blocking, orographic lifting, localized convergence and the diurnal heating cycle on the localized heavy rainfall will also be discussed.

The Mei-Yu Season

During late spring and early summer, the large-scale circulations over east Asia undergo two distinct changes (**Murakami, 1958**; **Yoshino, 1965**; **He et al., 1987**; and others). The first transition, in May, corresponds to the onset of the Southeast Asian monsoon when rains spread over Assam, the west coast of the Malay Peninsula, Indochina, and south China. The second transition occurs about one month later and corresponds to the onset of the Indian summer monsoon.

The onset of the Mei-Yu season over southern China and Taiwan (15 May–June 15) (**Chen, 1983**) occurs during the first transition and ends during the second transition. During TAMEX (Taiwan Area Mesoscale Experiment) 1987 (**Kuo and Chen, 1990**), the mean state from 10 May to June 27 is characterized by the presence of early summer monsoon trough over southern China (**Fig. 1**A) and prevailing southwesterly monsoon over southern China and Taiwan at the 850-hPa level between a permanent low-pressure center in the lee-

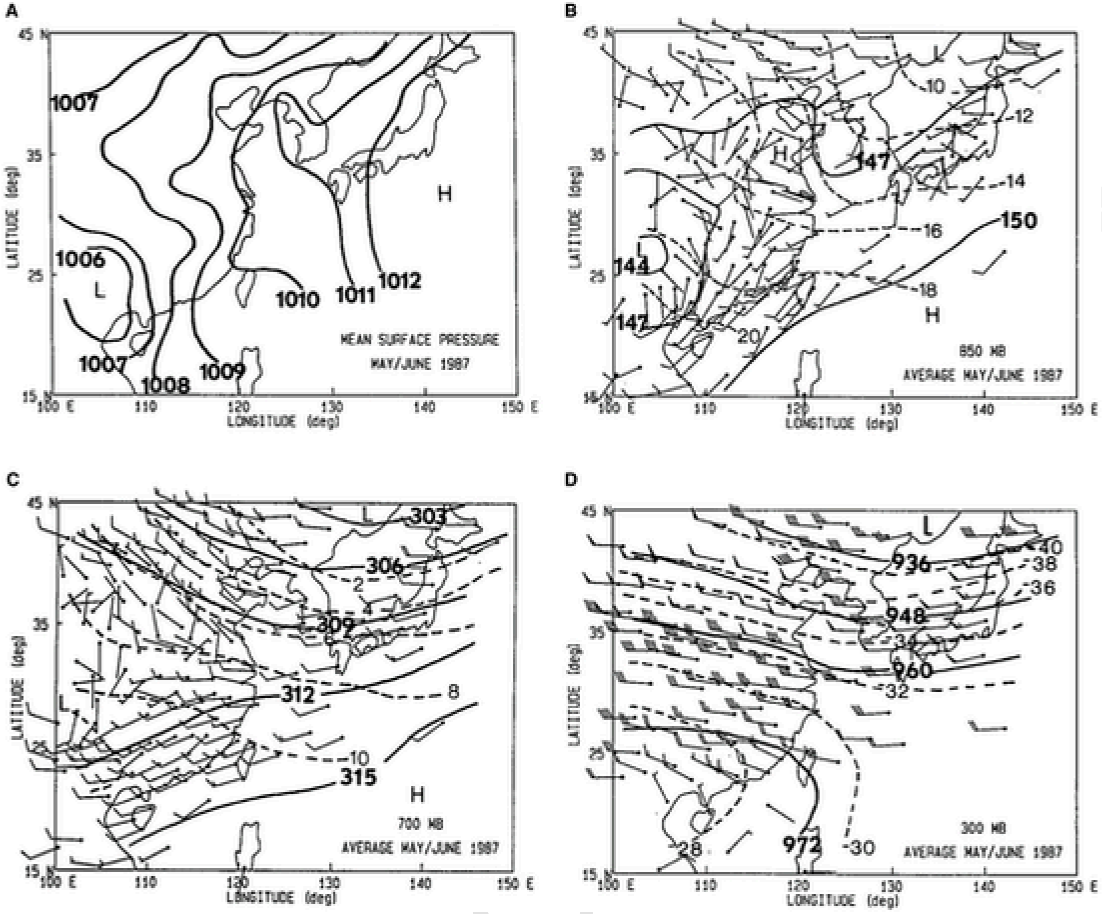

Fig. 1 The mean-state maps for the period from May 10 to June 27, 1987. Winds (m s^{-1}) with one pennant, full barb, and half-barb representing 25, 5, and 2.5 m s^{-1}, respectively. (A) The mean sea level pressure (hPa). (B) 850-hPa level. Geopotential height (solid) every 30 m; isotherms (dashed) every 2°C. (C) Same as (B), but for 700-hPa level. (D) 300-hPa level. Geopotential height (solid) every 120 m; isotherms (dashed) every 2°C. Source: **Chen (1993)**

side of the Tibetan Plateau and Northwest Pacific Subtropical High (NPSH) (**Fig. 1**B). At the 700-hPa level, the westerly current surrounds the Tibetan Plateau (**Fig. 1**C) with the South Asian anticyclone in upper levels (**Fig. 1**D).

During the second transition, the large-scale rain belt and Mei-Yu front move to the Yangtze River Valley, Korean Peninsula, and southwestern Japan with decreasing temperature gradients across the frontal zone over the China plain (**Chen, 1983**). Concurrently, the NPSH shifts northeastward with the prevailing southwesterly monsoon flow along the west/northwestern periphery of the NPSH. At the 300-hPa level, the westerly wind speed maximum moves to the north of the Tibetan Plateau. These changes are accompanied by a large temperature increase in the troposphere over the Afghanistan-Western Tibetan Plateau (**Murakami and Ding, 1982**), and the semiarid regions over northern China (**Kato, 1987**). **He et al. (1987)** emphasize the importance of the large-scale subsidence and warming induced by the elevated heat source over the Tibetan Plateau, which affect the large-scale circulation patterns. For TAMEX 1987, the second seasonal transition occurred around June 16. After the second seasonal transition, the upper-level westerlies as well as the baroclinic zone shifted north of the Tibetan Plateau (**Fig. 2**A and B). The tropospheric warming > 6 K over the China plain with a maximum exceeding 10 K in the semiarid region north of the Tibetan Plateau (**Fig. 2**C).

After the second transition in mid-June, the westerly current south of the Tibetan Plateau at the 300-hPa disappears with a westerly wind axis extending from Central Asia to Japan and easterlies to the south of 25°–30°N. In the meantime, the Tibetan high dominates the upper-level troposphere circulation patterns over the China plain with northeasterlies around the southern China coast and Taiwan (**Fig. 2**B). Over Japan, the westerly wind maximum remains in the same position as in winter (**Murakami, 1958**).

Because of the northward shift of the baroclinic zone and the westerly jet, the intrusion of polar cold air into the subtropics is unlikely, ending the early summer rainy season (or the Mei-Yu season) over southern China and Taiwan (**Chen, 1993**). In the meantime, the Mei-Yu season commences over the Yangtze River Valley (**Tao and Chen, 1987**) with decreasing thermal contrast across the frontal zone due to subsidence associated with the Tibetan High (**He et al., 1987**) and solar heating over the northern China plain (**Kato, 1987**). The

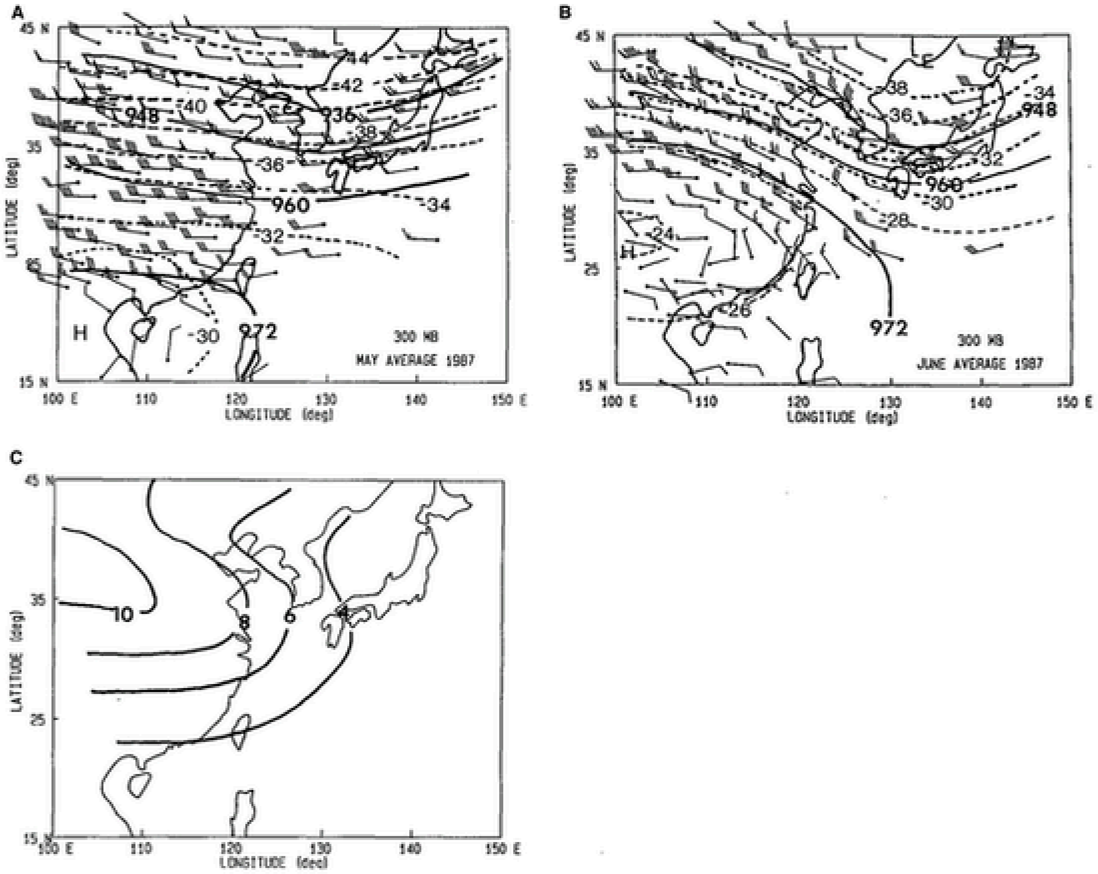

Fig. 2 (A) The mean 300-hPa-level map for the period of 10–31 May 1987. Winds (m s^{-1}) with one pennant, full barb, and half-barb representing 25, 5, and 2.5 m s^{-1}, respectively. Geopotential heights (solid) every 120 m; isotherms (dashed) every 2°C. (B) Same as (A), but for the period of 16–27 June 1987. (C) The temperature differences (°C) between the period of 10–31 May 1987 and 16–27 June 1987 at the 300-hPa level. Source: **Chen (1993)**

Baiu fronts summarized by **Ninomiya and Murakami (1987)** and the Changma over Korea (**Lee et al., 2017**) mainly occur at this stage.

Eastward Propagating Shortwave Trough and Lee Cyclogenesis

It is well known that the leeside of the major high mountains such as the Alps, Rocky Mountains, Tibetan Plateau, and others (**Zishka and Smith, 1980**; **Murakami and Huang, 1984**; **Chen et al., 1991**) are favorable locations for lee cyclogenesis. Before the second seasonal transition, with the westerly current surrounding the Tibetan Plateau, eastward propagating upper-level short-wave troughs embedded in the westerly current are common. An approaching eastward moving upper-level shortwave trough may lead to strengthening of the westerly flow over the Plateau, which results in cyclogenesis in the leeside (**Chen and Li, 1995a**; **Chen and Chen, 1995**). As the shortwave trough moves off the Tibetan Plateau, it merges with the lee trough, which leads to the subsequent deepening of the mesoscale Mei-Yu frontal cyclone (**Fig. 3**). **Murakami and Huang (1984)** identified six low-pressure systems embedded in the shear zone on the leeside of the Tibetan Plateau during the 1979 early summer rainy season. They suggested that these systems were excited by the mechanical effect of high mountains under the westerly current over the Tibetan Plateau.

The upper-level shortwave trough could also provide the upper-level baroclinic forcing for the development of heavy precipitation in the subtropics (**Chen and Li, 1995a**). In some cases, upper-level divergence occurs between weak northeasterlies in the southeastern quadrant of the South Asian anticyclone and westerlies/northwesterlies to the east, creates favorable conditions for deep convection in southern China and Taiwan (**Chen and Li, 1995a**; **Li et al., 1997**).

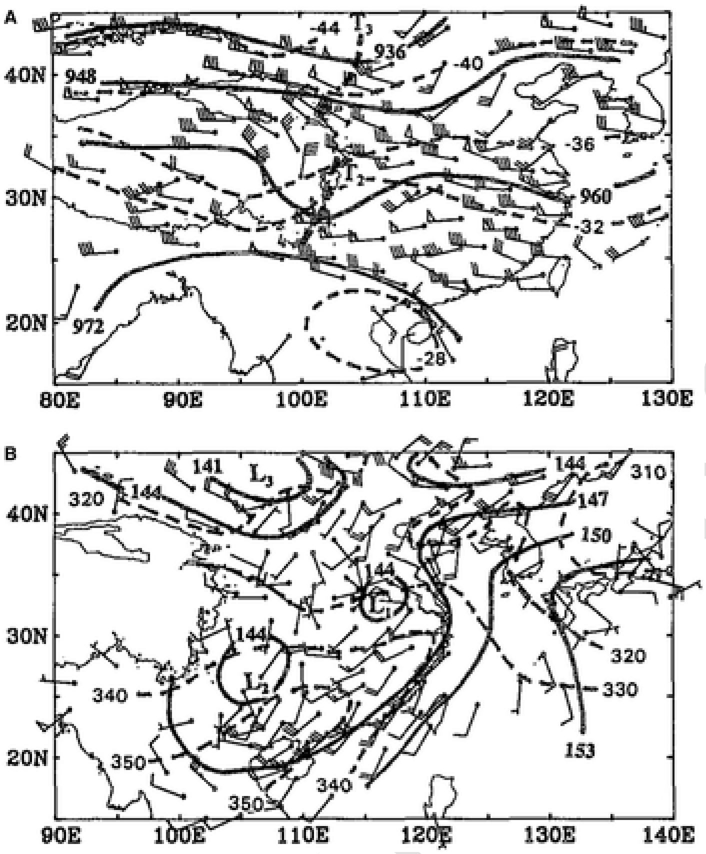

Fig. 3 Synoptic-scale charts for 0000 UTC May 21, 1987. (A) 300 hPa: geopotential heights (solid) every 120 m; isotherms (dashed) every 4°C. (B) 850 hPa: geopotential heights (solid) every 30 m; equivalent potential temperature (dashed) every 10°C. Winds (m s^{-1}) with one pennant, full barb, and half-barb representing 25, 5, and 2.5 m s^{-1}, respectively. Source: Chen and Li (1995a).

A Mid-latitude Trough North of the Tibetan Plateau

A mid-latitude trough embedded in the upper-level westerly jet north of the Tibetan Plateau frequently brings in cold polar air behind the trough into the China plain at low levels. This is achieved by the northerly wind component between the trough and the migrating high-pressure cell behind the trough (**Chen et al., 1989**, **2022a**, **b**; **Chen 1993**; and others). Five major Mei-Yu systems that passed northern Taiwan (13–14 May, 16–17 May, 26–27 May, 7–8 June, 14–15 June) during TAMEX were used in the composite analysis in **Fig. 4**. The synoptic evolution of these systems is very similar. For each frontal system, a stage (1 through 8) is assigned to each synoptic time period every 12 hours based on the 850-hPa wind shift line as well as surface frontal position along 120°E. At Stage 6, the Mei-Yu front reaches northern Taiwan. Stage 2 is approximately two days before Stage 6 whereas Stage 8 is approximately one day after. The southeastward advance of the 850-hPa Mei-Yu trough into the southern China coast and Taiwan is related to the southeastward advance of the migratory high behind the mid-latitude trough over northern China (**Fig. 4**) as revealed by individual case studies (**Chen et al., 1989**; **Chen and Hui, 1990**, **1992**; and others). Composited latitude-time sections along 120°E from the surface to the 300-hPa level as a function of stage is presented in **Fig. 5**. It is apparent that the southeastward movement of the Mei-Yu frontal system and the intrusion of cold, dry air from the north in low levels is closely linked to the passage of an upper-level mid-latitude trough over northern China as found in TAMEX case studies and recent studies (**Chen et al., 2022b**). Frontogenesis occurs when the northwesterly flow from mid-latitudes converges with the southwesterly monsoon flow from the subtropics west of the mesoscale Mei-Yu frontal cyclone (**Chen, 1993**; **Chen et al., 1994**).

If a blocking pattern is present in mid-latitudes, it could result in a slow southeastward movement of the Mei-Yu front (**Hsiao and Chen, 2014**; **Chen et al., 2018**). For a deep mid-latitude trough, the dynamic forcing associated with the upper-level jet could play an important role for the spin up of the Mei-Yu frontal cyclone in the subtropics (**Chen et al., 2022a**).

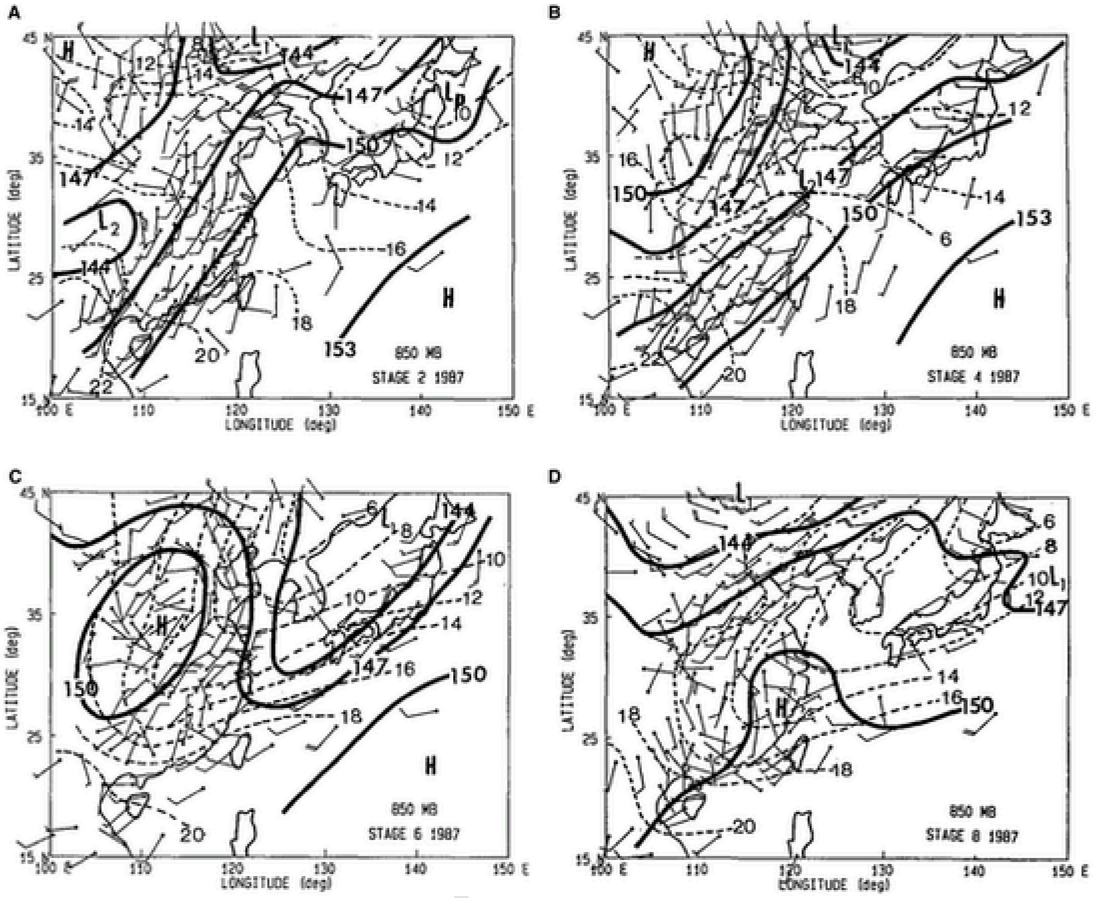

Fig. 4 Composited 850-hPa charts for (A) stage 2; (B) stage 4; (C) stage 6; (D) stage 8. Winds (m s^{-1}) with full barb and half-barb representing 5 and 2.5 m s^{-1}, respectively. Geopotential heights every 30 m (solid); isotherms every 2°C (dashed). Source: **Chen (1993)**

Mei-Yu Jet/Front Systems

Over southern China, the Mei-Yu fronts have a marked northward vertical tilt (**Fig. 6**) (**Chen et al., 1989**; **Chen and Hui, 1990**, **1992**; **Chen et al., 2018**, **2022b**; and others). The frontal slope is determined by the balance between the Coriolis acceleration and density difference (neglecting friction) across the front (**Margules, 1906**). The frontal slope is maintained under an equilibrium condition between the wind and density fields (**Palmen and Newton, 1969**). Because of the existence of the frontal slope, the passage of the 850-hPa trough over the Taiwan area frequently occurs up to 1–2 days after the passage of the surface front (**Chen and Li, 1995a**; **Tu et al., 2014**; and others).

All Mei-Yu frontal systems found during the Taiwan Area Mesoscale Experiment (TAMEX) (**Chen et al., 1989**; **Trier et al., 1990**; **Chen, 1993**; **Chen et al., 1994**, **1997**; and others) and recent studies (**Tu et al., 2014**; **Chen et al., 2018**; **Chen et al., 2022a**; and others) exhibit baroclinic characteristics: (i) appreciable temperature/moisture gradients in the lower troposphere; (ii) marked vertical tilt; (iii) upper-level jet/front system with tropopause folding; (iv) thermally direct circulation across the frontal zone; and (v) subsynoptic low-level jet (SLLJ) in the frontal zone ahead of the Mei-Yu trough (**Chen and Yu, 1988**; **Chen et al., 2005**) associated with the secondary circulation of the moist baroclinic jet/front system (**Chen et al., 1994**, **1997**; **Chen and Tseng, 2000**; **Chen and Chen, 2002**; **Du et al., 2014**). The SLLJ occurs between the 900- and 600-hPa levels (~1–4 km) due to the Coriolis force acting on the lower branch of the secondary circulation (**Chen et al., 1994**) and is enhanced by latent heat release as the Mei-Yu frontal cyclone deepens (**Chen et al., 1997**). The rising motion associated with the secondary circulations brings the warm, moist, high equivalent potential temperature air upward along the sloping frontal zone and provides the lifting mechanism for the development of precipitation in the frontal zone. A schematic diagram of the secondary circulation across the jet/front system is given in **Fig. 7**.

For a prolonged Mei-Yu frontal system during 10–15 June 1975 with a mid-latitude blocking pattern, the apparent temperature gradients across the surface front and associated upper-level jet/front were clearly evident (**Hsiao and Chen, 2014**) but not properly resolved

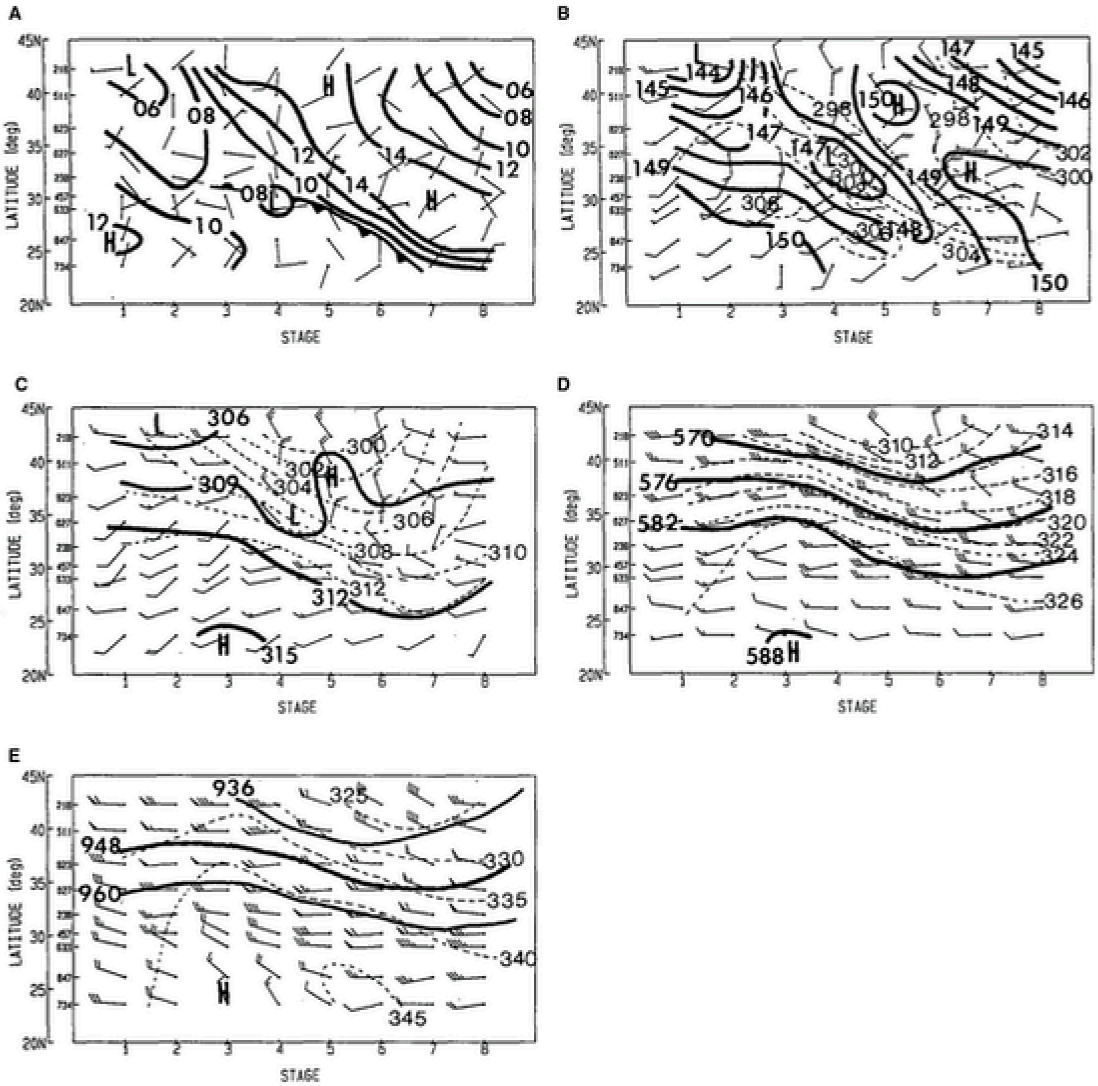

Fig. 5 Composited latitude-time sections along 120°E as a function of stage. Winds (m s^{-1}) with one pennant, full barb, and half-barb representing 25, 5, and 2.5 m s^{-1}, respectively. (A) Sea level pressure (hPa, *p*–1000). (B) 850-hPa level. Geopotential heights every 10 m (solid); potential temperature every 2 K (dashed). (C) 700-hPa level. Geopotential heights every 30 m (solid); potential temperature every 2 K (dashed). (D) 500-hPa level. Geopotential heights every 60 m (solid); potential temperature every 2 K (dashed). (E) 300-hPa level. Geopotential heights every 120 m (solid); potential temperature every 5 K (dashed). Source: **Chen (1993)**.

by the filtered and subjectively analyzed 240-km grid data using only four vertical levels (e.g., 850-hPa, 700-hPa, 500-hPa, and 400-hPa level) (**Chen and Chang, 1980**).

Moist Transport by the Southwesterly Monsoon Flow

Tu et al. (2019) studied the marine boundary layer jets (MBLJs) during the later period of the early summer rainy season of Taiwan in June for five years (2008–12) and examined their relationship with Mei-Yu heavy rainfall. The MBLJ occurs in the planetary boundary layer (PBL) below the inversion at the 900-hPa level (**Tu et al., 2019**, **2020**). The MBLJ develops when the Mei-Yu trough over southern China is more pronounced and the western Pacific subtropical high (WPSH) is stronger with the ridge axis extending further westward than normal (**Fig. 8**). In the MBLJ core, the vertical wind profile resembles an Ekman spiral with a wind speed maximum of more than 10 m s^{-1} in the PBL (**Tu et al., 2019**).

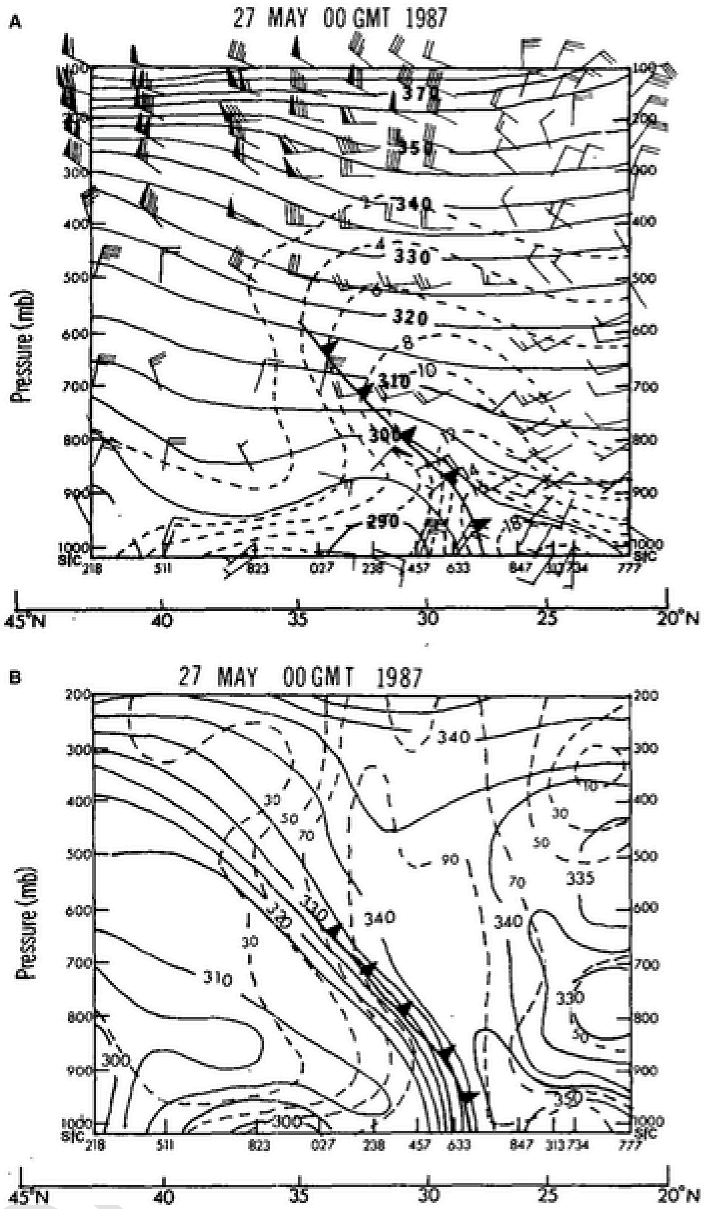

Fig. 6 North-south cross sections along 118°E for 0000 UTC May 27, 1987: (A) Potential temperature (solid) every 5 K; water vapor mixing ratio (dashed) every g kg^{-1} and winds in m s^{-1} with 1 pennant, full barb, and half barb denoting 25, 5, and 2.5 m s^{-1}, respectively. (B) Equivalent potential temperature (solid) every 5 K, and relative humidity (dashed) every 20%. Source: **Chen et al. (1989)**.

The MBLJ transports moisture from the northern South China Sea whereas the SLLJ provides the subsynoptic lifting needed to produce heavy Mei-Yu rainfall in the frontal zone (**Tu et al., 2019**, **2020**; **Chen et al., 2022a**). Furthermore, under favorable large-scale settings, orographic lifting of the southwesterly MBLJs by the Snow Mountains and/or the Central Mountain Range contributes to heavy rainfall over the southwestern slopes of these mountains and over southwestern Taiwan (**Fig. 9**). During 10–12 June 2012, the prefrontal southwesterly SLLJ and strong low-level winds associated with the MBLJ with large horizontal moisture fluxes (>360 g kg^{-1} m s^{-1} at the 950-hPa level) (**Chen et al., 2018**) are lifted by the southwestern slopes of the Snow Mountains and Central Mountain Range, which resulted in a three-day heavy orographic precipitation event with total rainfall accumulation of > 1000 mm and > 1500 mm, respectively (**Fig. 10**).

For the coastal heavy rainfall event during the Terrain-influenced Monsoon Rainfall Experiment (TiMREX) Intensive Observing Period (IOP) #8, a warm, moist south/southwesterly MBLJ is lifted by a ~ 500 m deep cold pool off the southwestern coast. The cold pool is caused by rain-evaporative cooling resulting from antecedent rains (**Xu et al., 2012**; **Tu et al., 2014**, **2017**). Above the cold pool, the south/southwesterly flow deflected by orographic blocking is nearly parallel to the Central Mountain Range (**Tu et al., 2014**). As a re-

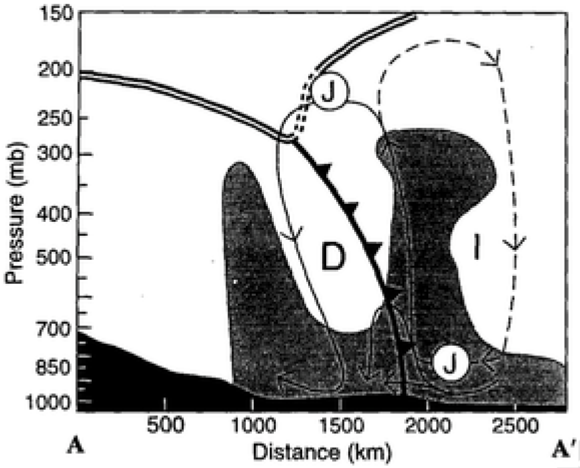

Fig. 7 Schematic delineating the secondary circulations across the jet/front system. The thin solid line depicts the strong direct (D) circulation. The thin dashed line depicts the weak indirect (I) circulation. The heavy solid line shows the low-level frontal position. The "J" indicates the upper-level and low-level jet positions. The double thin line shows the position of the tropopause. Regions with relative humidity greater than 70% are shaded. Source: **Chen et al. (1994)**.

sult, the heavy rainfall maximum occurs over the southwest coast of Taiwan, where the MBLJ converges with the offshore flow associated with the cold pool (**Xu et al., 2012**). The rain showers are enhanced by localized low-level convergence, drift inland, and then diminish.

Orographic Effects on Mei-Yu Fronts over the Southeastern China Coast and the Taiwan Area

As the Mei-Yu front penetrates into the subtropics, the depth of the postfrontal cold air decreases due to a decrease in the Coriolis parameter (**Chen et al., 1989**; **Chen and Hui, 1990**, **1992**). The shallow Mei-Yu front interacts with the hilly terrain along the southeastern China coast (**Fig. 11**A–C) and the terrain over Taiwan (**Chen and Hui, 1990**, **1992**; **Trier et al., 1990**). The postfrontal cold air is ducted around the southeastern China coast and moves rapidly southward with a pressure ridge along the coast with strong northeasterlies blowing down the pressure gradients (**Fig. 11**).

In the vicinity of Taiwan, the microscale structure of the leading edge of the cold front resembles a density current as observed by instrumented aircraft (**Chen and Hui, 1990**). The microscale structure of the cold front cannot be resolved by mesoscale models with a grid spacing on the order of 15 km (**Sun and Chern, 2006**). The Mei-Yu front is shallow with a depth of ~ 1 km and cut into two branches by the Central Mountain Range, with a local pressure ridge along the northeastern coast of Taiwan (**Chen et al., 1989**; **Chen and Hui, 1990**, **1992**; **Trier et al., 1990**). The postfrontal northeasterlies were blocked by the terrain and do not reach the southwestern leeside area. After the frontal passage, relatively low pressure occurs over the southwestern plain hydrostatically (**Chen and Hui, 1990**) from the cold air behind the front not reaching the southwestern plain, while surrounding areas experience rising pressure with the arrival of the cold air.

In addition to front-terrain interaction, orographic blocking of the southwesterly flow by the Central Mountain Range occurs in the prefrontal region with a windward ridge-leeside trough pressure pattern. A mesolow forms over the southeastern coast due to the southwesterly flow aloft, moves over the mountains, and descends adiabatically (**Fig. 11**A and B) (**Chen et al., 1989**; **Chen and Hui, 1990**, **1992**; **Sun et al., 1991**). The barrier jet (BJ; **Chen and Li, 1995a,b**; **Li and Chen, 1998**) off or along the northwest Taiwan coast is a result of orographic blocking of the prefrontal southwesterly flow by the island terrain (**Fig. 12**). The significant Lagrangian flow acceleration of the northern branch of the deflected airflow along the northwest coast is driven by the pressure gradient force as the airflow moves down the orographically induced pressure ridge along the windward coast (**Yeh and Chen, 2003**). The observed and simulated wind BJ has a wind speed maximum at the top of the mixed layer (~1 km) due to frictional retardation in the lowest levels (**Li and Chen, 1998**; **Yeh and Chen, 2003**). Within the mixed layer, the alongshore force balance is a three-way balance between inertial advection, pressure gradient force, and frictional force (**Yeh and Chen, 2003**). The BJ is strongest when the surface windward ridge-leeside trough pressure pattern is most pronounced. Furthermore, the simulated BJ also exhibits diurnal variations with an early morning maximum, which is approximately ~ 3 m s^{-1} stronger than the afternoon minimum (**Lin et al., 2011**). The location and strength of the orographically induced low-level strong winds along the northwest coast of Taiwan also depend on the impinging angle and wind speed of the prevailing winds (**Yeh and Chen, 2003**). A schematic for the BJ formation is given in **Fig. 13**.

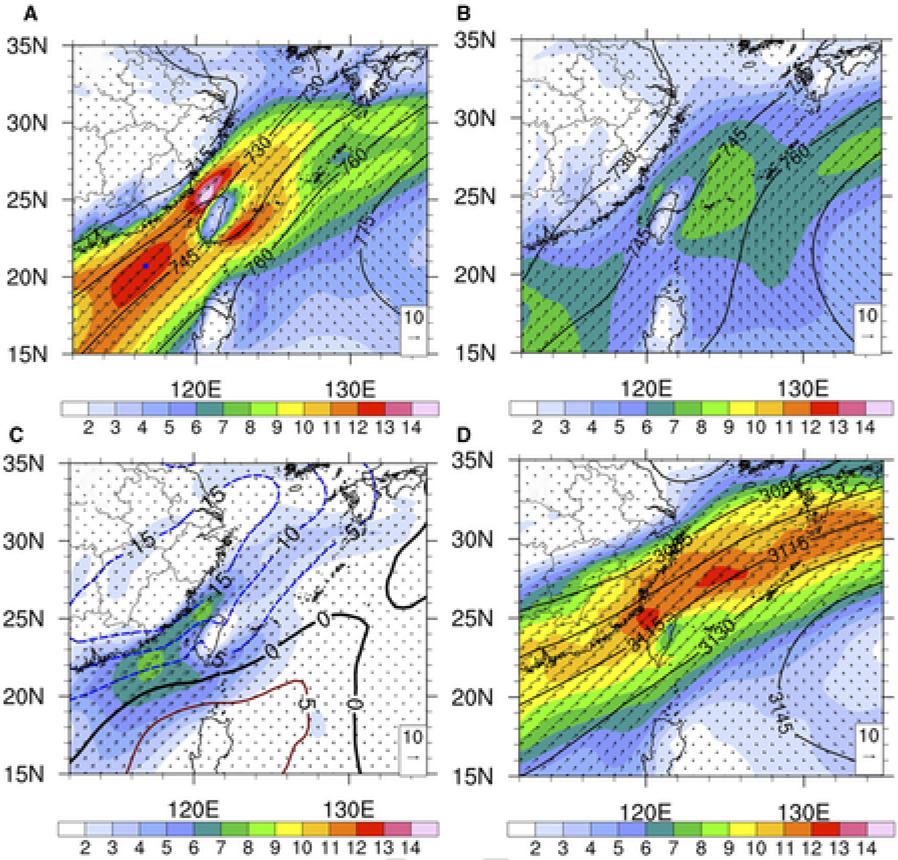

Fig. 8 The 2008–12 Climate Forecast System Reanalysis (CFSR) (A) composite of the 925-hPa winds (V; m s^{-1}) and geopotential height (gpm) for the MBLJ days. (B) June monthly mean 925-hPa winds (V; m s^{-1}) and geopotential height (gpm). (C) The 925-hPa winds (V; m s^{-1}) and geopotential height (gpm) differences between the MBLJ days and the June monthly mean (MBLJ days V − monthly mean V). (D) As in (A), but for the 700-hPa winds (V; m s^{-1}) and geopotential height (gpm). Blue solid circle in (A) marks Dongsha Island. Source: **Tu et al. (2019)**

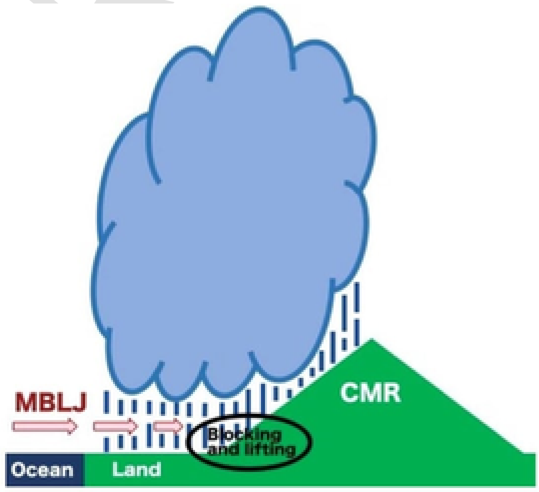

Fig. 9 A schematic diagram showing the moisture transport from the Northern South China Sea (NSCS) toward Taiwan and rising motion due to flow deceleration, blocking, and lifting by the Central Mountain Range (CMR). Source: **Chen et al. (2022a)**

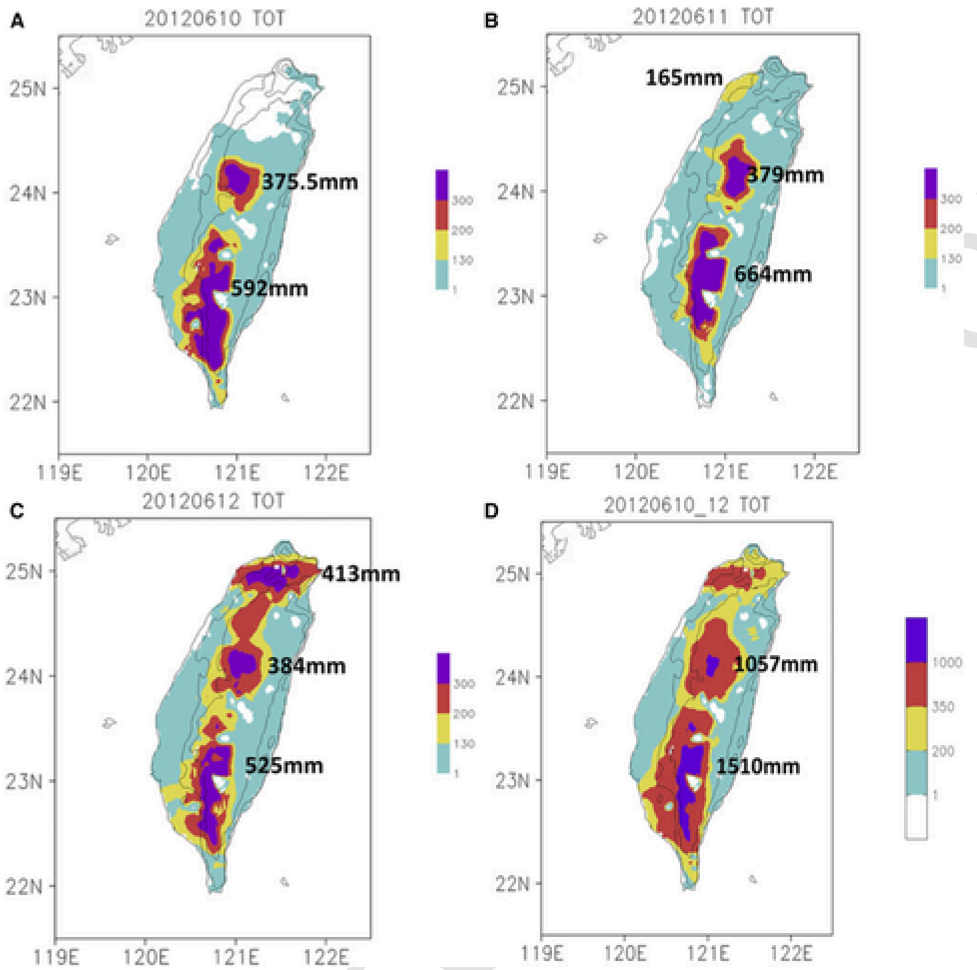

Fig. 10 (A) Daily (0000–2400 LST) rainfall accumulation (mm; color shaded) for 10 June 2012. (B) As in (A), but for 11 June. (C) As in (A), but for 12 June. (D) Rainfall accumulation (mm) during 10–12 June. Terrain contours are 100 and 500 m. Source: **Chen et al. (2018)**

Front Terrain Interactions and the Occurrences of Localized Heavy Rainfall

Along the northwestern coastal plain, about 80% of the rainfall during TAMEX is associated with the passage of surface fronts (**Yeh and Chen, 1998**). The convergence between the BJ and southwest monsoon flow, and/or frontal wind shift line, leads to the development of localized heavy rainfall over northwestern Taiwan (**Li et al., 1997**; **Yeh and Chen, 2002**; **Chen et al., 2018**; **Ke et al., 2019**). Moreover, the BJ transports abundant moisture locally to the convergence area from the south, which contributes to enhanced heavy coastal precipitation over western/northwestern Taiwan (**Li et al., 1997**; **Kerns et al., 2010**). In the absence of a SLLJ, the BJ could develop due to orographic blocking of the MBLJ. A notable example occurred during the TiMREX IOP #8 (**Tu et al., 2017**).

Chen et al. (2018) studied the interaction between a Mei-Yu jet/front system and topography for a heavy rainfall event over northern Taiwan during 11–12 June 2012. The total rainfall accumulation over the northwestern Taiwan coast is ~ 435 mm, and ~ 477 mm within the Taipei Basin (**Fig. 14**). From 2200 LST 11 June to 0200 LST 12 June (**Fig. 14**B–D), the rainfall maximum along the northwestern coast is closely related to the arrival of scattered prefrontal echoes, followed by the ENE–WSW-oriented convective line associated with the Mei-Yu front. The convective activity over the northwestern coast is enhanced by the localized convergence between the southerly BJ and the postfrontal west-northwesterly flow. The slow-moving Mei-Yu front is deep (~1.5 km) due to a blocking pattern in the mid-latitudes. From 0200–0800 LST 12 June (**Fig. 14**D–G), the relatively deep postfrontal cold air moved over the Yang-Ming Mountains (with peaks ~ 1120 m) and stalled in the Taipei Basin for 6 h with heavy rainfall there. Also, as the Mei-Yu front/850-hPa trough arrived over northern Taiwan, the postfrontal northwesterlies behind the trough impinged on the northwestern slopes of the Snow Mountains, which resulted in heavy rainfall (**Fig. 14**H).

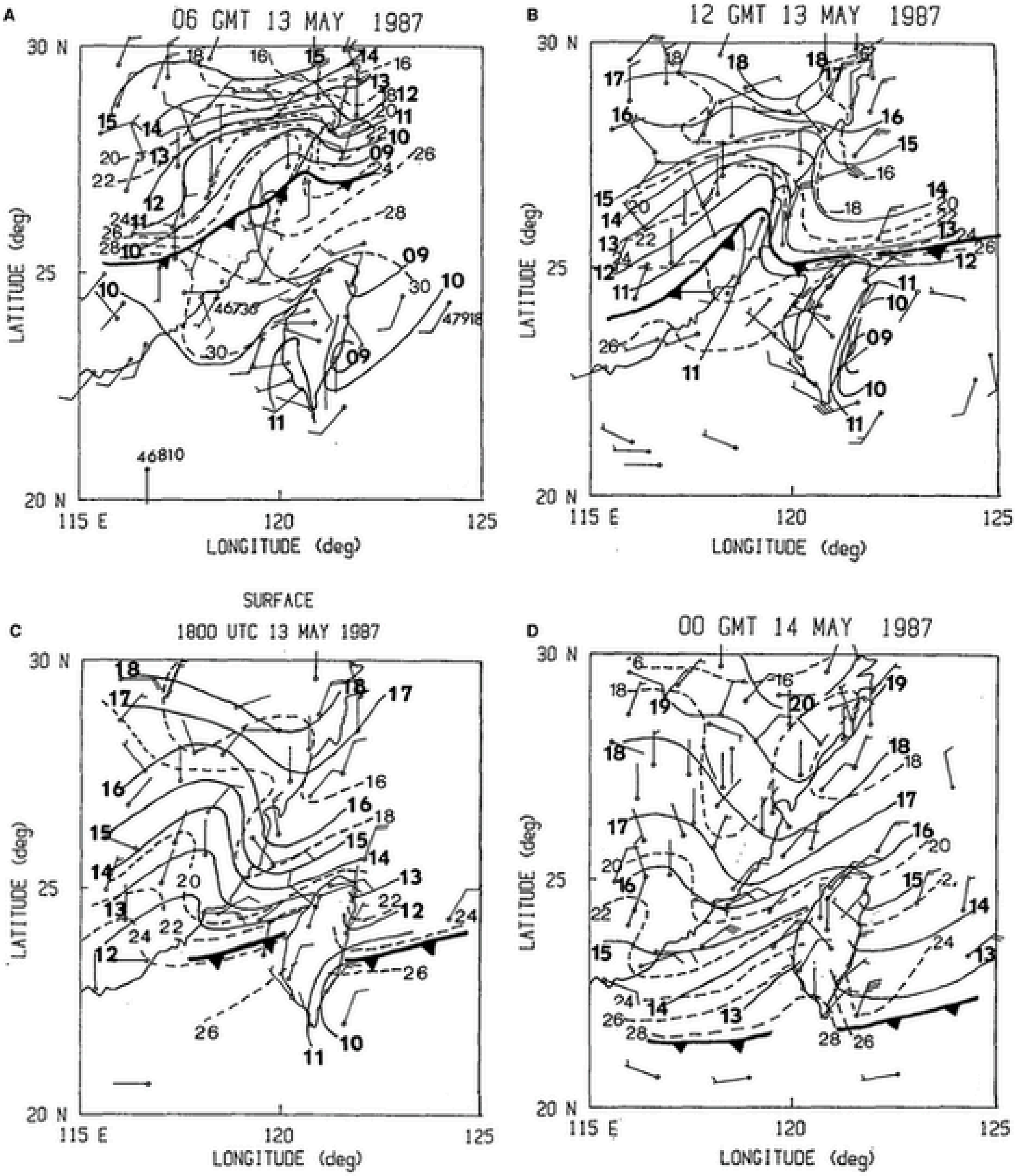

Fig. 11 Regional surface maps. Ship reports were included in the analysis. Winds (m s^{-1}) with full barb and half-barb representing 5 and 2.5 m s^{-1}, respectively. Sea level pressure (solid) every 1 mb (millibars–1000); isotherms (dashed) every 2°C. (A) 0600 UTC 13 May (1400 LST 13 May) 1987. (B) 1200 UTC 13 May (2000 LST 13 May) 1987. (C) 1800 UTC 13 May (0200 LST 14 May) 1987. (D) 0000 UTC 14 May (0800 LST 14 May) 1987. Source: **Chen and Hui (1992)**.

Tu et al. (2022) studied a very shallow, east–west-oriented Mei-Yu front (<1 km) that arrived the northern coast of Taiwan in the early morning of June 2, 2017. It is unable to move over the Yang-Ming Mountains when it first arrives and is anchored along the northern side of the Yang-Ming Mountains for 8 h (0200–1000 LST). In addition, the southwesterly barrier jet with maximum winds in the 900–950-hPa layer brings in abundant moisture and converges with the northwesterly flow in the southwestern flank of the Mei-Yu frontal cyclone. This resulted in torrential rain (>600 mm) falling over the northern side of the Yang-Ming Mountains during the period (**Fig. 15**A–F). The postfrontal cold northerly flow at the surface is deflected by the Yang-Ming Mountains and moves through the Keelung River and Tamsui River valleys into the Taipei basin. From 1100–1200 LST, with the gradual deepening of the postfrontal cold air, the front finally passes over the Yang-Ming Mountains and arrives at the Taipei basin, resulting in an east–west-oriented rainband with the rainfall maxima

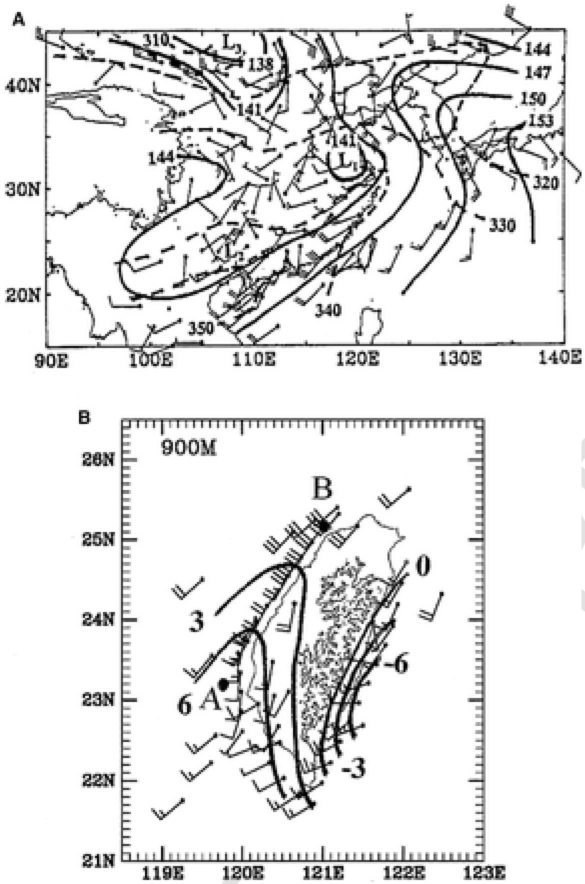

Fig. 12 (A) Subjectively analyzed synoptic-scale chart at 850 hPa for 1200 UTC May 21, 1987. (B) Winds and D values at the 900-m level around 1500 UTC 21 May. Geopotential heights (A) every 30 m; D values every 3 m. Winds ($m\ s^{-1}$) with one pennant, full barb, and half barb represent 25, 5, and 2.5 $m\ s^{-1}$, respectively. The horizontal wind field in (B) is constructed from rawinsonde, pibal, and aircraft data during 1330–1720 UTC May 21, 1987. Terrain contours are 1.5 km. Source: **Li and Chen (1998)**.

over the northwestern coast and Taipei basin (**Fig. 15**G). From 1300–1400 LST, the frontal rainband continues to move southward with rainfall over the northwestern slopes of the Snow Mountains (**Fig. 15**H).

Chen and Chen (2003) show that the horizontal distributions of climatological rainfall patterns for different rainfall regimes are strongly dependent on the direction of the low-level prevailing flow, with much higher rainfall on the windward side. During TAMEX, the orographic lifting of the moisture-laden southwesterly monsoon flow results in rainfall maxima on the southwestern slopes of the Snow Mountains and the Central Mountain Range (**Yeh and Chen, 1998**). About 50% of the rainfall on the southwestern windward slopes occurs as scattered orographic showers during non-frontal periods (**Fig. 16**) with significant diurnal variations. TAMEX results and recent studies show that most of the rainfall there occurs in the afternoon hours due to the development of sea breezes/anabatic winds (**Yeh and Chen, 1998**; **Kerns et al., 2010**; **Chen et al., 2007**; **Tu et al., 2014**). The timing of the maximum hourly rainfall incidences on the lower windward slopes occurs 1–2 h earlier than on the upper slopes and mountain interior (**Yeh and Chen, 1998**; **Kerns et al., 2010**). For the May 31, 2008 case during TiMREX, after a shallow surface front passes central Taiwan, heavy rainfall occurs over the southwestern windward slopes in the afternoon hours (**Tu et al., 2017**). The orographic lifting of the prevailing warm, moist, west-southwesterly flow aloft, combined with a sea breeze–upslope flow at the surface provides the localized lifting needed for the development of heavy precipitation. These results demonstrate that in the absence synoptic disturbances, diurnal and local effects are important in determining the location and timing of the occurrences of localized heavy rainfall during the early summer rainy season over Taiwan.

Conclusions

This article gives an overview of the seasonal, large-scale, synoptic, mesoscale, and island-scale circulations and front-terrain interactions during the Mei-Yu season over Taiwan.

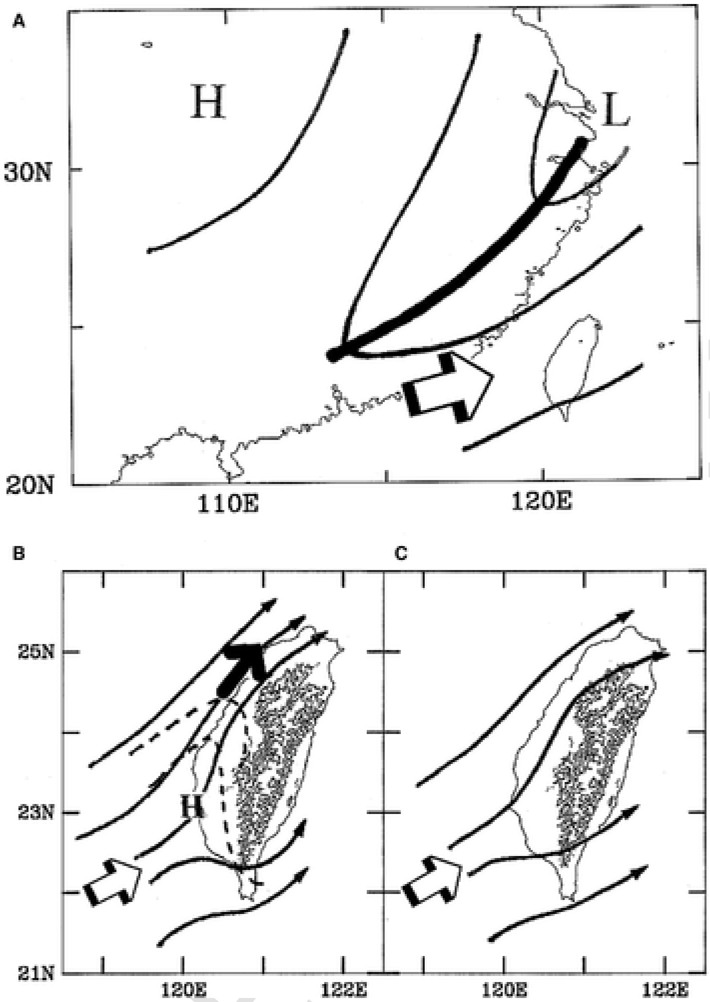

Fig. 13 A schematic diagram for the barrier jet formation. (A) The large-scale low-level flow pattern, (B) the mesoscale airflow near the 1-km level, and at (C) 2.5-km level over the Taiwan area are shown. The heavy line, open arrow, and heavy arrow represent the low-level pressure trough, upstream southwesterly flow, and barrier jet, respectively. The distribution for the geopotential height in (A), local sea level pressure pattern (dashed) in (B) and streamlines (solid) in (B) and (C) are also shown. Terrain contours are 1.5 km. Source: Li and Chen (1998).

The onset of the Mei-Yu season over Taiwan coincides with the onset of the southeast Asia monsoon with a broad westerly wind zone surrounding the Tibetan Plateau and southern China at the 500-hPa level. It ends when the baroclinic zone shifts northward and the upper-level Tibetan High, with northeasterlies/easterlies around the southern China coast and the Taiwan area, is established. When the westerly current prevails over the Tibetan Plateau, lee cyclogenesis frequently occurs over southern China behind the high mountains.

During the passage of a mid-latitude trough, these lee cyclones frequently move eastward and deepen between the cold northerly wind component behind the mid-latitude trough and the warm, moist southwesterly monsoon from the south. The Mei-Yu jet/front over southern China exhibits baroclinic characteristics with thermally direct circulation across the frontal zone. Widespread heavy rainfall over the Taiwan area is likely due to moisture transport from the northern South China Sea to Taiwan by the MBLJ below the 850-hPa level, which develops due to an increase in the pressure gradients between the deepening Mei-Yu trough and the westward extension and/or strengthening of the North Pacific Subtropical High.

The depth of the postfrontal cold air decreases as the Mei-Yu front penetrates to the subtropics and is ∼1 km over the Taiwan area. Front-terrain interactions, orographic lifting of the southwesterly flow, and local circulations during the diurnal cycle affect the timing and location of localized heavy precipitation.

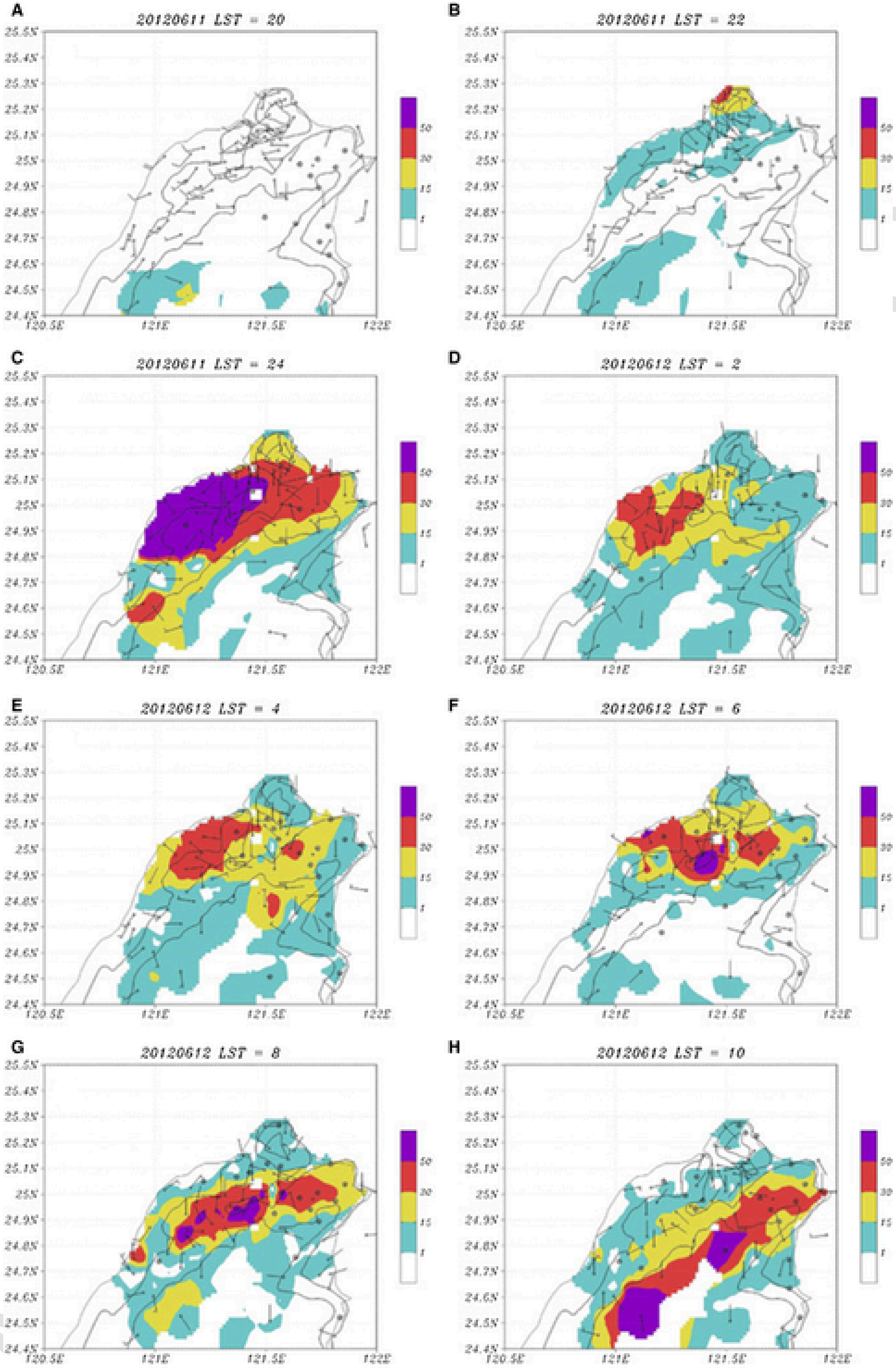

Source: **Chen et al. (2018)**

Fig. 14 Hourly rainfall (mm) and surface winds (one full barb and half barb represent 5 and 2.5 m s^{-1}, respectively) over northern Taiwan: (A) 2000 and (B) 2200 LST 11 June 2012; (C) 0000, (D) 0200, (E) 0400, (F) 0600, (G) 0800, and (H) 1000 LST 12 June 2012. Terrain contours are 100 and 500 m, respectively.

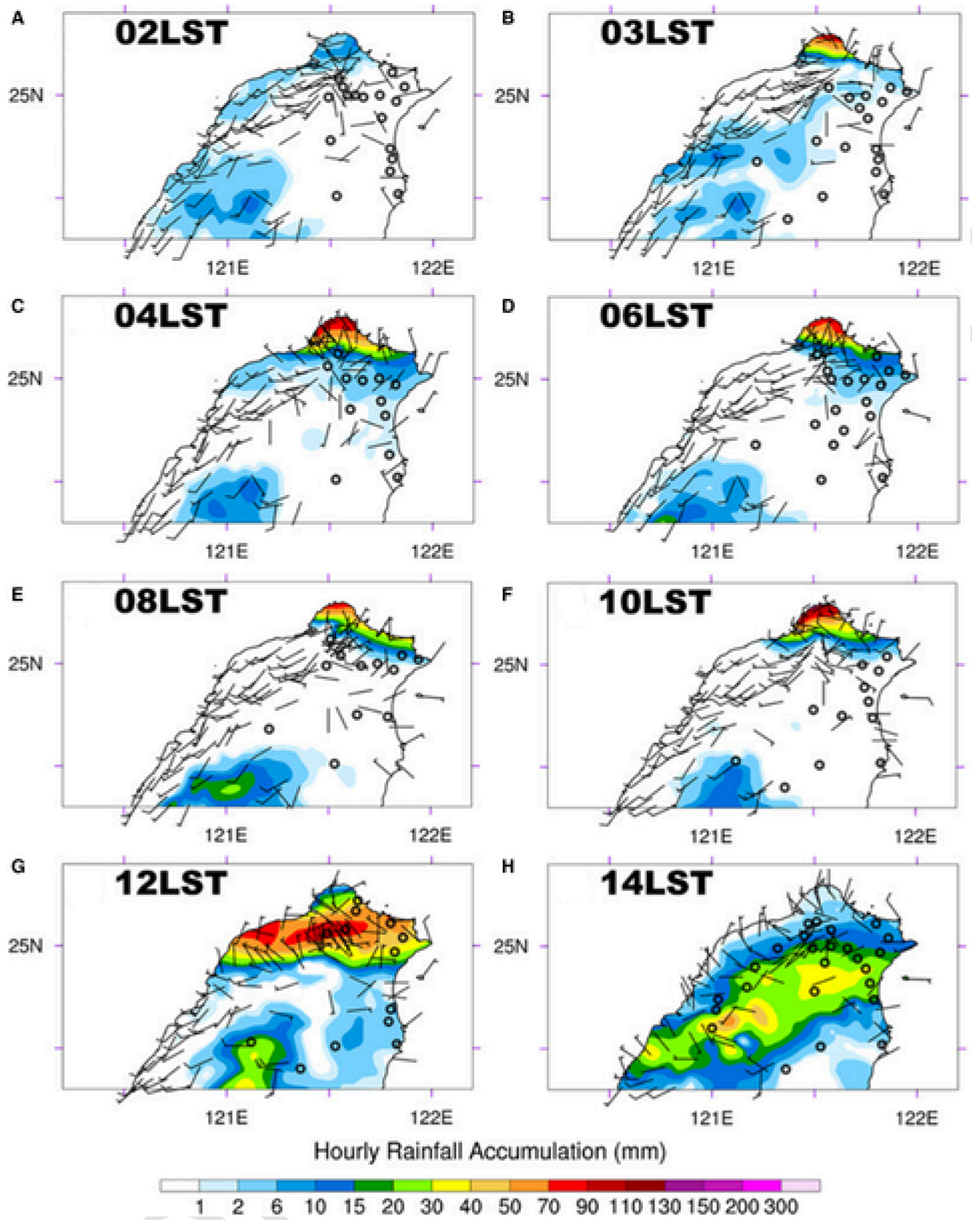

Fig. 15 The observed station surface winds (m s^{-1}; one full barb represents 5 m s^{-1}) and hourly rainfall accumulation (mm; color shaded) from rain gauges ending at (A) 0200 LST June 2, 2017, (B) 0300 LST June 2, 2017, (C) 0400 LST June 2, 2017, (D) 0600 LST June 2, 2017, (E) 0800 LST June 2, 2017, (F) 1000 LST June 2, 2017, (G) 1200 LST June 2, 2017, and (H) 1400 LST June 2, 2017. Source: **Tu et al. (2022)**.

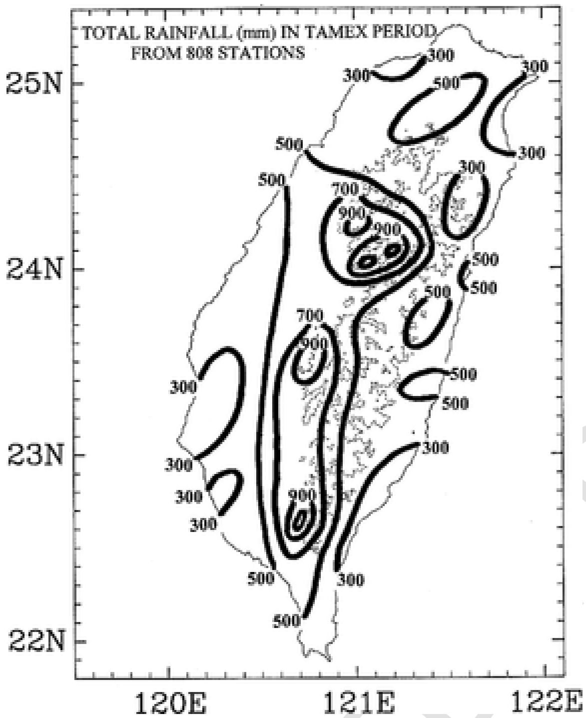

Fig. 16 Total rainfall distribution during 10 May–27 June 1987 from 808 daily rainfall stations. Contours start at 300 mm with 200-mm intervals. Source: **Yeh and Chen (1998)**.

References

Chen, C.-S., Chen, Y.-L., 2003. The rainfall characteristics of Taiwan. Mon. Weather Rev. 131, 1323–1341. doi:10.1175/1520-0493(2003)131<1323:TRCOT>2.0.CO;2.

Chen, C.-S., Chen, Y.-L., Liu, C.-L., Lin, P.-L., Chen, W.-C., 2007. Statistics of heavy rainfall occurrences in Taiwan. Weather Forecast. 22, 981–1002. doi:10.1175/WAF1033.1.

Chen, G.T.-J., Chang, C.-P., 1980. The structure and vorticity budget of an early summer monsoon trough (Mei-Yu) over southeastern China and Japan. Mon. Weather Rev. 108, 942–953. doi:10.1175/1520-0493(1980)108<0942:TSAVBO>2.0.CO;2.

Chen, G.T.-J., 1983. Observational aspects of the Mei-Yu phenomenon in subtropical China. J. Meteorol. Soc. Jpn. 61, 306–312. doi:10.2151/jmsj1965.61.2_306.

Chen, G.T.-J., Yu, C.-C., 1988. Study of low-level jet and extremely heavy rainfall over northern Taiwan in the Mei-Yu season. Mon. Weather Rev. 116, 884–891. doi:10.1175/1520-0493(1988)116<0884:SOLLJA>2.0.CO;2.

Chen, G.T.-J., Wang, C.-C., Lin, D.T.-W., 2005. Characteristics of low-level jets over northern Taiwan in Mei-Yu season and their relationship to heavy rain events. Mon. Weather Rev. 133, 20–43. doi:10.1175/MWR-2813.1.

Chen, S.-J., Kuo, Y.-H., Zhang, P.-Z., Bai, Q.-F., 1991. Synoptic climatology of cyclogenesis over east Asia. Mon. Weather Rev. 119, 1407–1418. doi:10.1175/1520-0493(1991)119<1407:SCOCOE>2.0.CO;2.

Chen, X.A., Chen, Y.-L., 1995. Development of low-level jets during TAMEX. Mon. Weather Rev. 123, 1695–1719. doi:10.1175/1520-0493(1995)123<1695:DOLLJD>2.0.CO;2.

Chen, X.A., Chen, Y.-L., 2002. Kinetic energy budgets of the low-level jet during TAMEX IOP 5. J. Meteorol. Soc. Jpn. 80, 1–19. doi:10.2151/jmsj.80.1.

Chen, Y.-L., Zhang, Y.-X., Hui, N.B.-F., 1989. Analysis of a surface front during the early summer rainy season over Taiwan. Mon. Weather Rev. 117, 909–931. doi:10.1175/1520-0493(1989)117<0909:AOASFD>2.0.CO;2.

Chen, Y.-L., Hui, N.B.-F., 1990. Analysis of a shallow front during the Taiwan area mesoscale experiment. Mon. Weather Rev. 118, 2649–2667. doi:10.1175/1520-0493(1990)118<2649:AOASFD>2.0.CO;2.

Chen, Y.-L., Hui, N.B.-F., 1992. Analysis of a relatively dry front during the Taiwan area mesoscale experiment. Mon. Weather Rev. 120, 2442–2468. doi:10.1175/1520-0493(1992)120<2442:AOARDF>2.0.CO;2.

Chen, Y.-L., 1993. Some synoptic-scale aspects of the surface fronts over southern China during TAMEX. Mon. Weather Rev. 121, 50–64. doi:10.1175/1520-0493(1993)121<0050:SSSAOT>2.0.CO;2.

Chen, Y.-L., Chen, X.A., Zhang, Y.-X., 1994. A diagnostic study of the low-level jet during TAMEX IOP 5. Mon. Weather Rev. 122, 2257–2284. doi:10.1175/1520-0493(1994)122<2257:ADSOTL>2.0.CO;2.

Chen, Y.-L., Li, J., 1995a. Large-scale conditions favorable for the development of heavy rainfall during TAMEX IOP3. Mon. Weather Rev. 123, 2978–3002. doi:10.1175/1520-0493(1995)123<2978:LSCFFT>2.0.CO;2.

Chen, Y.-L., Li, J., 1995b. Characteristics of surface airflow and pressure patterns over the island of Taiwan during TAMEX. Mon. Weather Rev. 123, 695–716. doi:10.1175/1520-0493(1995)123<0695:COSAAP>2.0.CO;2.

Chen, Y.-L., Chen, X.A., Chen, S., Kuo, Y.-H., 1997. A numerical study of the low-level jet during TAMEX IOP 5. Mon. Weather Rev. 125, 2583–2604. doi:10.1175/1520-0493(1997)125<2583:ANSOTL>2.0.CO;2.

Chen, Y.-L., Tseng, S.-F., 2000. Comments on “The intensification of the low-level jet during the development of mesoscale convective systems on a Mei-Yu front”. Mon. Weather Rev. 128, 495–506. doi:10.1175/1520-0493(2000)128<0495:COTIOT>2.0.CO;2.

Chen, Y.-L., Chu, Y.-J., Chen, C.-S., Tu, C.-C., Teng, J.-H., Lin, P.-L., 2018. Analysis and simulations of a heavy rainfall event over northern Taiwan during 11–12 June 2012. Mon. Weather Rev. 146, 2697–2715. doi:10.1175/MWR-D-18-0001.1.

Chen, Y.-L., Wang, C.-K., Tu, C.-C., Hsiao, F., Lin, P.-L., 2022a. Revisiting a Mei-Yu front associated with heavy rainfall over Taiwan during 6–7 June 2003. Atmosphere 13 (5), 644. doi:10.3390/atmos13050644.

Chen, Y.-L., Tu, C.-C., Hsiao, F., Chen, C.-S., Lin, P.-L., Lin, P.-H., 2022b. An overview of low-level jets (LLJs) and their roles in heavy rainfall over the Taiwan area during the early summer rainy season. Meteorology 1 (1), 64–112. doi:10.3390/meteorology1010006.

Du, Y., Zhang, Q., Chen, Y.-L., Zhao, Y., Wang, X., 2014. Numerical simulations of spatial distributions and diurnal variations of low-level jets in China during early summer. J. Clim. 27, 5747–5767. doi:10.1175/JCLI-D-13-00571.1.

He, H., McGinnis, J.M., Song, Z., Yanai, M., 1987. Onset of the Asian summer monsoon in 1979 and the effect of the Tibetan Plateau. Mon. Weather Rev. 115, 1966–1995. doi:10.1175/1520-0493(1987)115<1966:OOTASM>2.0.CO;2.

Hsiao, F., Chen, Y.-L., 2014. Revisiting the structure and characteristics of an early summer monsoon trough over South China in 1975. Sci. Lett. Atmos. 10, 194–198. doi:10.2151/sola.2014-041.

Kato, K., 1987. Airmass transformation over the semiarid region around North China and abrupt change in the structure of the Baiu front in early summer. J. Meteorol. Soc. Jpn. 65, 737–750. doi:10.2151/jmsj1965.65.5_737.

Ke, C.-Y., Chung, K.-S., Wang, T.-C.C., Liou, Y.-C., 2019. Analysis of heavy rainfall and barrier-jet evolution during Mei-Yu season using multiple Doppler radar retrievals: a case study on 11 June 2012. Tellus A Dyn. Meteorol. Oceanogr. 71, 1–21. doi:10.1080/16000870.2019.1571369.

Kerns, B.W.J., Chen, Y.-L., Chang, M.-Y., 2010. The diurnal cycle of winds, rain, and clouds over Taiwan during the Mei-Yu, summer, and autumn rainfall regimes. Mon. Weather Rev. 138, 497–516. doi:10.1175/2009MWR3031.1.

Kuo, Y.-H., Chen, G.T.-J., 1990. The Taiwan area mesoscale experiment (TAMEX): an overview. Bull. Am. Meteorol. Soc. 71, 488–503. doi:10.1175/1520-0477(1990)071<0488:TTAMEA>2.0.CO;2.

Lee, J.-Y., Kwon, M., Yun, K.-S., Min, S.-K., Park, I.-H., Ham, Y.-G., Jin, E.K., Kim, J.-H., Seo, K.-H., Kim, W., Yim, S.-Y., Yoon, J.-H., 2017. The long-term variability of Changma in the East Asian summer monsoon system: a review and revisit. Asia Pac. J. Atmos. Sci. 53, 257–272. doi:10.1007/s13143-017-0032-5.

Li, J., Chen, Y.-L., Lee, W.-C., 1997. Analysis of a heavy rainfall event during TAMEX. Mon. Weather Rev. 125, 1060–1082. doi:10.1175/1520-0493(1997)125<1060:AOAHRE>2.0.CO;2.

Li, J., Chen, Y.-L., 1998. Barrier jets during TAMEX. Mon. Weather Rev. 126, 959–971. doi:10.1175/1520-0493(1998)126<0959:BJDT>2.0.CO;2.

Lin, P.-L., Chen, Y.-L., Chen, C.-S., Liu, C.-L., Chen, C.-Y., 2011. Numerical experiments investigating the orographic effects on a heavy rainfall event over the northwestern coast of Taiwan during TAMEX IOP 13. Meteorol. Atmos. Phys. 114, 35–50. doi:10.1007/s00703-011-0155-7.

Margules, M., 1906. Über Temperaturschichtung in stationär bewegter und in ruhender Luft. Hann-Band. Meteor. Z., 243–254. [Translated and edited by Volken E, Giesche A, and Brönnimann S (2016) On temperature stratification in resting and non-accelerated moving air. Meteorol. Z. 25, 795–804. doi:10.1127/metz/2016/0833.

Murakami, T., 1958. The sudden change of upper westerlies near the Tibetan Plateau at the beginning of summer monsoon. J. Meteorol. Soc. Jpn. 36, 239–247. doi:10.2151/jmsj1923.36.6_239.

Murakami, T., Ding, Y.-H., 1982. Wind and temperature changes over Eurasia during the early summer of 1979. J. Meteorol. Soc. Jpn. 60, 183–196. doi:10.2151/jmsj1965.60.1_183.

Murakami, T., Huang, W.-G., 1984. Orographic effects of the Tibetan Plateau on the rainfall variations over Central China during the 1979 summer. J. Meteorol. Soc. Jpn. 62, 895–909. doi:10.2151/jmsj1965.62.6_895.

Ninomiya, J., Murakami, T., 1987. The early summer rainy season (Baiu) over Japan. In: Chang, C.-P., Krishnamurti, T.N. (Eds.), Monsoon Meteorology. Oxford University Press, pp. 93–121.

Palmen, E., Newton, C.W., 1969. Atmospheric Circulation Systems. Academic Press, p. 603.

Sun, W.-Y., Chern, J.-D., Wu, C.-C., Hsu, W.-R., 1991. Numerical simulation of mesoscale circulation in Taiwan and surrounding area. Mon. Weather Rev. 119, 2558–2573. doi:10.1175/1520-0493(1991)119<2558:NSOMCI>2.0.CO;2.

Sun, W.-Y., Chern, J.-D., 2006. Numerical study of the influence of Central Mountain ranges in Taiwan on a cold front. J. Meteorol. Soc. Jpn. 84, 27–46. doi:10.2151/jmsj.84.27.

Tao, S., Chen, L., 1987. A review of recent research on the East Asia summer monsoon in China. In: Chang, C.-P., Krishnamurti, T.N. (Eds.), Monsoon Meteorology. Oxford University Press, pp. 60–92.

Trier, S.B., Parsons, D.B., Matejka, T.J., 1990. Observations of a subtropical cold front in a region of complex terrain. Mon. Weather Rev. 118, 2449–2470. doi:10.1175/1520-0493(1990)118<2449:OOASCF>2.0.CO;2.

Tu, C.-C., Chen, Y.-L., Chen, C.-S., Lin, P.-L., Lin, P.-H., 2014. A comparison of two heavy rainfall events during the Terrain-influenced Monsoon Rainfall Experiment (TiMREX) 2008. Mon. Weather Rev. 142, 2436–2463. doi:10.1175/MWR-D-13-00293.1.

Tu, C.-C., Chen, Y.-L., Chen, S.-Y., Kuo, Y.-H., Lin, P.-L., 2017. Impacts of including rain-evaporative cooling in the initial conditions on the prediction of a coastal heavy rainfall event during TiMREX. Mon. Weather Rev. 145, 253–277. doi:10.1175/MWR-D-16-0224.1.

Tu, C.-C., Chen, Y.-L., Lin, P.-L., Du, Y., 2019. Characteristics of the marine boundary layer jet over the South China Sea during the early summer rainy season of Taiwan. Mon. Weather Rev. 147, 457–475. doi:10.1175/MWR-D-18-0230.1.

Tu, C.-C., Chen, Y.-L., Lin, P.-L., Lin, P.-H., 2020. The relationship between the boundary layer moisture transport from the South China Sea and heavy rainfall over Taiwan. Terr. Atmos. Ocean Sci. 31, 159–176. doi:10.3319/TAO.2019.07.01.01.

Tu, C.-C., Chen, Y.-L., Lin, P.-L., Huang, M.-Q., 2022. Analysis and simulations of a heavy rainfall event associated with the passage of a shallow front over northern Taiwan on 2 June 2017. Mon. Weather Rev. 150, 505–528. doi:10.1175/MWR-D-21-0113.1.

Xu, W., Zipser, E.J., Chen, Y.-L., Liu, C., Liou, Y.-C., Lee, W.-C., Jou, B.J.-D., 2012. An orography-associated extreme rainfall event during TiMREX: initiation, storm evolution, and maintenance. Mon. Weather Rev. 140, 2555–2574. doi:10.1175/MWR-D-11-00208.1.

Yeh, H.-C., Chen, Y.-L., 1998. Characteristics of rainfall distributions over Taiwan during Taiwan area mesoscale experiment (TAMEX). J. Appl. Meteorol. Climatol. 37, 1457–1469. doi:10.1175/1520-0450(1998)037<1457:CORDOT>2.0.CO;2.

Yeh, H.-C., Chen, Y.-L., 2002. The role of offshore convergence on coastal rainfall during TAMEX IOP 3. Mon. Weather Rev. 130, 2709–2730. doi:10.1175/1520-0493(2002)130<2709:TROOCO>2.0.CO;2.

Yeh, H.-C., Chen, Y.-L., 2003. Numerical simulations of the barrier jet over northwestern Taiwan during the Mei-Yu season. Mon. Weather Rev. 131, 1396–1407. doi:10.1175/1520-0493(2003)131<1396:NSOTBJ>2.0.CO;2.

Yoshino, M.M., 1965. Four stages of the rainy season in early summer over East Asia (Part I). J. Meteorol. Soc. Jpn. 43, 231–245. doi:10.2151/jmsj1965.43.5_231.

Zishka, K.M., Smith, P.J., 1980. The climatology of cyclones and anticyclones over North America and surrounding ocean environs for January and July, 1950–77. Mon. Weather Rev. 108, 387–401. doi:10.1175/1520-0493(1980)108<0387:TCOCAA>2.0.CO;2.